Theoretical Insight into the Fluorescence Spectral Tuning Mechanism: A Case Study of Flavin-dependent Bacterial Luciferase

Xiaodi Fu[a], Wenwen Diao[b], Yanling Luo[c], Yajun Liu[a,d], and Zhanfeng Wang[a]*

[a] Dr. X. Fu, Prof. Z. Wang, and Prof. Y. Liu, Center for Advanced Materials Research, Beijing Normal University, Zhuhai 519087, China

Email: zfwang@bnu.edu.cn

[b] Dr. W. Diao, Oujiang Laboratory (Zhejiang Lab for Regenerative Medicine, Vision and Brain Health), Wenzhou 325000, China

[c] Dr. Y. Luo, School of Chinese Materia Medica, Tianjin University of Traditional Chinese Medicine, Tianjin 301617, China

[d] Prof. Y. Liu, Key Laboratory of Theoretical and Computational Photochemistry, Ministry of Education, College of Chemistry, Beijing Normal University, Beijing 100875, China

KEYWORDS: bacterial luciferase • spectral tuning • electric field effect • electrostatic effect • QM/MM • TD-DFT

ABSTRACT: Bioluminescence of bacteria is widely applied in biological imaging, environmental toxicants detection, and many other situations. Understanding the spectral tuning mechanism not only helps explain the diversity of colors observed in nature, but also provides principles for bioengineering new color variants for practical applications. In this study, time-dependent density functional theory (TD-DFT) and quantum mechanics and molecular mechanics (QM/MM) calculations have been employed to understand the fluorescence spectral tuning mechanism of bacterial luciferase, with a focus on the electrostatic effect. The spectrum can be tuned by both the homogeneous dielectric environment and oriented external electric fields (OEEFs). Increasing solvent polarity leads to a redshift of the fluorescence emission maximum, λ_F, accompanied by an increase in density. In contrast, applying an OEEF along the long axis of the isoalloxazine ring leads to a significant red- or blue-shift in λ_F, depending on the direction of the OEEF, but with negligible changes in its intensity. The effect of polar solvents is directionless, and the red-shifts can be attributed to the larger dipole moment of the S_1 state compared to the S_0 state. However, the effect of OEEFs directly correlates with the difference dipole moment between the S_1 and S_0 states, which is directional and determined by the charge redistribution upon excitation. Moreover, the electrostatic effect of bacterial luciferase is in line with the presence of an internal electric field (IEF) pointing in the negative *X* direction with a magnitude of ca. 30 MV/cm. Finally, key residues that contribute to this IEF and strategies for modulating the spectrum through site-directed point mutations are discussed.

Introduction

Bioluminescence is a widespread light-emitting phenomenon of living organisms, ranging from bacterial, fungal, insect, and marine creatures.[1-5] Due to its simple operation, short detection time, and high sensitivity, bioluminescence has been extensively used in many fields, such as biological analysis,[6] bioimaging,[6-9] detection of environmental toxicants,[10-13] and many others.[2, 4, 14-18] However, its application is somewhat limited by the fact that the photon energy is weakened by the scattering and absorption of biological tissue. To further improve its spectroscopic properties and expand its applications, an in-depth understanding of its spectral tuning mechanism is highly desired.[19]

Bioluminescent bacteria are the most widely distributed bioluminescent species in the world. The bioluminescence found in bacteria is a result of the activity of the luciferase enzyme, known as bacterial luciferase. Bacterial luciferase is a unique flavin-dependent monooxygenase, utilizing reduced flavin mononucleotide ($FMNH_2$), O_2, and a long-chain aliphatic aldehyde to produce visible light.[20-22] Previous NMR studies have demonstrated that the luciferase-bound $FMNH_2$ molecule adopts an anionic form ($FMNH^-$, I-1).[23] $FMNH^-$ can activate a dioxygen molecule to form 4a-hydroperoxy-5-hydro-FMN (HFOOH, I-2) with the assistance of a proton supplier.[23-25] HFOOH further reacts with the aliphatic aldehyde, yielding the 4a-peroxyhemiacetal-5-hydro-FMN species (HFOOCH(OH)R, I-3).[26-28] Decomposition of I-3 generates the 4a-hydroxy-5-hydro-FMN intermediate in its first singlet excited state $^1HFOH^*$ (I-4),[20] which is responsible for light emission. I-4 returns to its ground state (HFOH, I-5) after radiative decay.[29] Finally, HFOH can rapidly convert to the oxidized flavin mononucleotide (FMN) species via a dehydration reaction, which can be further transformed to $FMNH^-$ to initiate another luminescence process.[30]

HFOH exhibits a fluorescence peak around 490 nm when bound in the active site of the luciferase protein.[30] However, it is unstable and readily converts to FMN with the loss of one water molecule in solution, as shown in **Scheme 1**. Consequently, N(5)-alkylated 4a-hydroxy flavins are commonly used as experimental models to mimic HFOH. Interestingly, the N5-alkylated analogs display weak fluorescence in solution, yet their fluorescence is greatly enhanced when bound to the enzymatic binding pocket.[31] Additionally, the fluorescence quantum yield was found to be markedly enhanced in a frozen state of solvents than at room temperature.[32-33] A joint computational and experimental study indicated that an orthogonal out-of-plane distortion of the terminal pyrimidine ring leads to the excited state deactivation via a conical intersection (CI) mediated internal conversion.[33] The geometry confinement imposed by the frozen solvent or the protein cavity restraints the ring distortion and blocks the CI-mediated internal conversion, readily explaining the fluorescence enhancement.[33-34]

Scheme 1. The proposed bioluminescence process of bacterial luciferase. R′ denotes $CH_2(CH_2OH)^3PO_4H_2$.

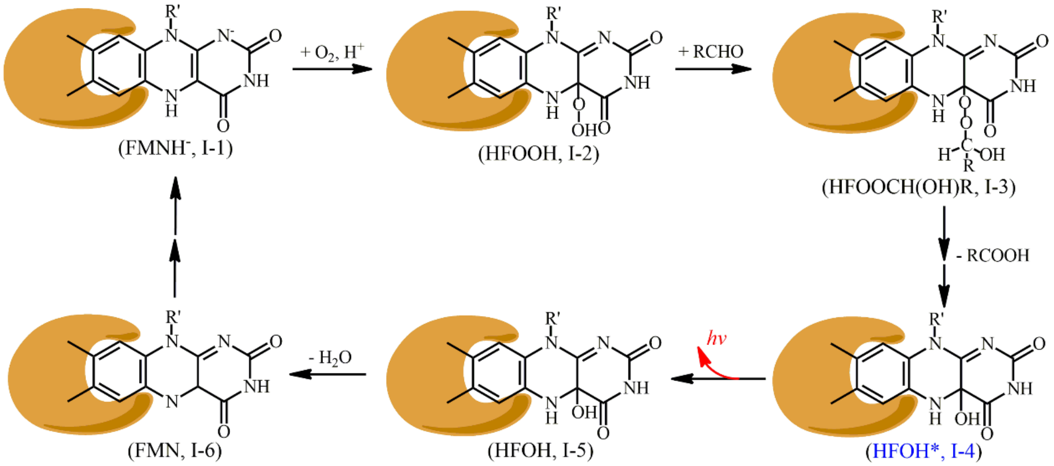

In addition to the geometry confinement exerted mainly by steric effects, the electrostatic interactions with the protein environment may play a key role in the modulation of photophysical and photochemical properties of chromophores.[19] Indeed, an increasing number of recent studies have shown that proteins not only provide cavities for their substrates but also modulate reactivity and reaction selectivity through electrostatic interactions with substrates.[35-49] In green fluorescent protein (GFP) and its mutants, the electrostatic environments imposed by different proteins were found to play key roles in spectral modulation.[50-54] Similarly, among the species of fireflies and their analogous beetles, it has been well-established that the effect of the electrostatic environments is the main factor in the emission color-tuning mechanism. [36, 55-56] Mutant firefly luciferases can yield different colors by inducing different local electric fields around the luciferin.[57-60] Therefore, it is important to gain an in-depth understanding of the electrostatic effect in bacterial luciferase system. The elucidation of this question will contribute to the rationalization of the color modulation mechanism in luciferase and fluorescent proteins caused by amino acid mutations or pH changes, and to their rational design to emit light at specific wavelengths.

In this work, we seek to understand how the fluorescence spectrum is modulated by the protein environment of bacterial luciferase, especially focusing on the effect of the electrostatic interaction with the fluorophore, HFOH. The effects of the protein environment on the fluorescence spectroscopic properties can be obtained by comparing the spectrum calculated on the fluorophore embedded in the protein environment (System I) to the corresponding spectrum calculated on the bare fluorophore using the vacuum-optimized geometry (System II) and the in-protein structure (System III). Specifically, comparison of the results of the bare fluorophore in Systems II and III gives the indirect effect of the protein surroundings through induced structural changes in the chromophore, while the direct electrostatic contributions can be obtained by the comparison of results between Systems I and III. Besides, we systematically investigate the spectroscopic properties of LFOH (4a-hydroxy-5-hydro-lumiflavin), a simplified model molecule of HFOH, in various solvents and in oriented external electric fields (OEEFs) to get an in-depth understanding of the spectral tuning mechanism in bacterial luciferase. In line with previous studies,[33-34] the indirect effect, i.e. geometry confinement by the steric effect of the protein environment, is found to be fundamental to its fluorescence efficiency. On the other hand, the electrostatic effect is found to play key roles in the fine-tuning of the spectrum, including emission maximum λ_F and intensity. Intriguingly, we find that the electrostatic effect of bacterial luciferase can be attributed to an internal electric field (IEF) pointing toward the negative F_X direction (from the pyrimidine ring to the xylene moiety) with a magnitude of ca. 30 MV/cm.

Computational Methods

Setup of System I: The crystallographic structure of *vibrio harveyi* luciferase (PDB ID: 3FGC)[61] was utilized for model construction. The structure comprises two heterodimers, 1 and 2, each containing two homologous subunits, α and β, with flavin mononucleotide (FMN) binding to the α-subunit of heterodimer 1. For the sake of computational efficiency, only heterodimer 1, including chains A and B, was retained in the model. The missing residues (residue IDs: 284-289) in chain A were added using the SWISS-MODEL[62] online server (available at: swissmodel.expasy.org). Since the missing residues (residue IDs: 319-332) in chain B are located at the end of the chain and are far away from the fluorophore, they were reasonably ignored. The FMN in the crystal structure was modeled as HFOH. The protonation states of titratable residues (histidine, glutamic acid and aspartic acid) were determined using the online PDB2PQR[63-65] program (available at: server.poissonboltzmann.org) in combination with the careful visual inspection of local hydrogen-bonded networks. All glutamic acid and aspartic acid residues were deprotonated. Histidine 45 in chain A and histidine 45 in chain B were doubly protonated, while the histidine residues 61, 82, 199, 215, 224, 234, and 249 in chain A and residues 29, 81, 82, 132, 145, 161, 209, and 224 in chain B were protonated at the ε position, histidine residues 44, 150, and 285 in chain A and residues 76 and 215 in chain B were protonated at the δ position. The Amber ff19SB force field[66] was employed for canonical protein residues, while the general amber force field (GAFF)[67] was used to describe HFOH. Charge parameters of HFOH were obtained from the RESP method[68] at the HF/6-31G* level with Gaussian 16.[69] The parmchk2 utility from AmberTools was used to generate missing parameters. Sodium ions were added to the protein surface to neutralize the overall charge of the systems. The resulted system was solvated in a rectangular box of TIP3P[70] waters extending up to a minimum cutoff of 12 Å from the protein surface.

Molecular dynamics (MD) simulations of System I. After proper setup, the system was then equilibrated in the following manner: (a) energy minimized using a combination of the steepest descent and conjugate-gradient methods; (b) heated up from 0 K to 300 K in NVT ensemble for 300 ps with a weak constraint of 25 kcal•mol^{-1}•Å^{-2} on the protein backbone atoms; (c) density equilibrated for 1 ns to achieve a uniform density at a target temperature of 300 K and a target pressure of 1.0 atm using an isothermal−isobaric Langevin thermostat[71] and Berendsen barostat[72] with a collision frequency of 2 ps^{-1} and a pressure relaxation time of 1 ps; (d) further equilibrated for 3 ns under the NPT ensemble with restraints removed to obtain a well-settled pressure and temperature. Finally, a 100 ns production MD simulation was performed. Nonbonded interactions were treated with Particle Mesh Ewald[73] method with a cutoff of 12 Å. Covalent bond containing hydrogen atoms were constrained using the SHAKE[74] algorithm to enable an integration step of 2 fs. All MD simulations were performed with the GPU version of the Amber 22 package.[75-77]

Quantum mechanics and molecular mechanics (QM/MM) calculations. The final equilibrated geometry from the production MD trajectory was used as the initial input structure for the QM/MM calculations. QM/MM calculations were performed using ChemShell software,[78] combining ORCA[79-80] for the QM region and DL_POLY[81-82] for the MM region with the AMBER force field. The QM/MM system contains the whole protein, counterions, and solvation water molecules within 8 Å of the protein. To include the polarizing effect of the MM region on the QM region, the electronic embedding scheme was employed in the QM/MM calculations.[83] The time-dependent DFT (TD-DFT)[84] method was employed for the QM region in excited state calculations. According to previous studies[20, 29], the frontier molecular orbitals of HFOH mainly localize in the isoalloxazine ring and are not affected by the ribose phosphate side-chain. Therefore, only the lumiflavin group was included in the QM region to reduce computational cost without loss of accuracy, while other atoms were placed in the MM region. A hydrogen link atom with the charge-shift model was applied to treat the QM/MM boundary. Considering the charge transfer character of the first excited S_1 state[20] and the well reproduction of the experimental fluorescence emission maximum (refer to Table S1),[30] the Coulomb-attenuated hybrid exchange-correlation functional CAM-B3LYP[85], which combines the features of the B3LYP functional with long-rang corrections using Hartree-Fock exchange, was used for the excited state calculations of the QM region. Geometry optimization of HFOH in its first excited S_1 state were calculated using a small basis set of 6-31+G** (labeled B1), with the residues within 6 Å of the chromophore in the MM region allowed to relax during the optimization process. The fluorescence spectroscopic properties were calculated with a larger basis set of def2-TZVP (labeled B2). Besides the method of CAM-B3LYP/def2-TZVP, four other functionals (B3LYP,[86-87] M06-2X,[88] ωB97X-D3,[89] and PBE0[90]) and three other basis sets (6-31+G**, 6-311+G**, and 6-311++G**) were tested, which were summarized in Table S1. The fluorescence wavelength greatly depends on the choice of the functional, yet it is not sensitive to the choice of basis set.

QM calculations. To ensure computational accuracy and efficiency, a simplified model of HFOH (4a-hydroxy-5-hydro-lumiflavin, denoted as LFOH) was used in QM calculations, where the ribose phosphate group was replaced with a methyl group (**Scheme 2**). The geometry of bare LFOH in its first excited state, used in System II, was optimized under vacuum using the TD-DFT method[84] with the range separated CAM-B3LYP functional and the 6-31+G** basis set, at the same level for the QM region used in QM/MM calculations. The geometry used in System III was the QM/MM-optimized bare LFOH structure that accounted for the steric effects of the protein surroundings. The spectroscopic properties of LFOH, including emission energy E_F, oscillator strength f, permanent dipole moment ($\boldsymbol{\mu}$) of the S_0 and S_1 states, and transition dipole moment $\boldsymbol{\mu}_{01}$, were determined at the TD-CAM-B3LYP/def2-TZVP level, which is same with that used for QM region in QM/MM calculations. Vertical excitation energies were considered, ignoring vibronic effects. The effect of solvent polarity was investigated with System III using the polarizable continuum model (PCM)[91-92] with five solvents (toluene, chlorobenzene, ethanol, DMSO, and water) covering a range of dielectric constant (ε).

Scheme 2. Illustration of the cartesian axes used in the present study, along with atom labels. *X*-axis points from N_{10} to N_1, while *Z*-axis points from N_{10} to N_5. *Y*-axis is perpendicular to the *X*-*Z* plane and points outward.

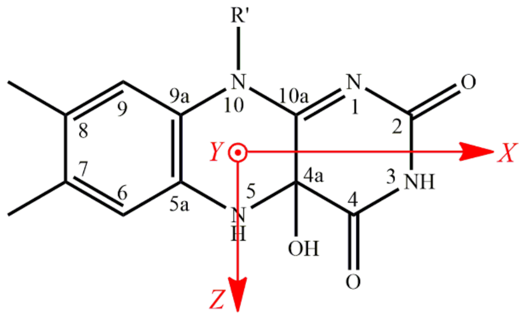

HFOH: R' = $CH_2(CHOH)_3OPO_3H_2$ LFOH: R' = CH_3

The effects of oriented external electric fields (OEEFs) were studied with System III using the planar QM/MM-optimized bare LFOH structure. The OEEFs were applied using the "Field = *M* ± *N*" keyword in Gaussian 16, which defines the axis of the electric fields, its direction along that axis (*M*) and its magnitude (*N* a.u., 1 a.u. = 5140 MV/cm). The short axis of isoalloxazine ring pointing from N_{10} to N_5 was defined as the *Z*-axis and the long axis pointing from N_{10} to N_1 was defined as the *X*-axis. (refer to **Scheme 2**). A range of moderate electric field strengths (F) between -0.0075 a.u. and 0.0075 a.u. were explored. A strong OEEF may change the energy order of the frontier orbitals of LFOH, which complicates the elucidation of the effect of OEEFs. It is noteworthy that the positive direction of the electric field vector is defined from the negative to the positive charge in Gaussian 16, which is opposite to the conventional definition in physics. To be consistent with the common sense of physics, the direction of the external electric field has been inverted in related discussions. The discussion of the effect of OEEFs are based on the results obtained using the TD-DFT/def2-TZVP method with the CAM-B3LYP functional.

Most of QM calculations were performed with Gaussian 16 software.[69] To exclude the influence of different software and make a direct assessment of the electrostatic effect of protein environment, we performed an additional QM calculation with System III in the gas phase using ORCA.[79-80] The emission energy difference obtained with different software is 0.09 eV (refer to Table S2), which is much smaller compared to the large difference (0.58 eV) caused by the protein environment. Figures were prepared with Multifwn,[93] VMD,[94] and PyMol.[95]

Results and Discussion

1. Geometry confinement by the protein environment. As alluded to above, the luciferase protein affects the emission properties of the chromophore either by modifying its geometry or through electrostatic interactions. To understand how the geometry of the light-emitter (HFOH) is influenced by the protein, we optimized its first excited state (S_1) geometry both in the protein environment (System I) and in the gas phase (System II), as shown in Figure 1A and 1B, respectively. The geometry embedded in the protein was calculated using the QM/MM method at the TD-CAM-B3LYP/6-31+G**//MM level, while the gas-phase geometry was optimized with the TD-DFT method at the TD-CAM-B3LYP/6-31+G** level. Notably, a simplified model of HFOH, denoted as LFOH, was used in the QM calculations, where the ribose phosphate group was replaced by a methyl group, to ensure computational accuracy and efficiency (refer to **Scheme 2**).[20, 29] In the presence of the protein environment (System I), the isoalloxazine ring adopts a more planar conformation, with a C_9-N_{10}-C_{10a}-N_1 dihedral angle of 147.6° (Figure 1A). The vertical energy difference between the S_1 and S_0 states (E_F) estimated at the TD-CAM-B3LYP/def2-TZVP//MM level is 2.52 eV, corresponding to an emission maximum (λ_F) of 493 nm, which is close to the experimentally determined value of ca. 490 nm.[30] In contrast, the optimized geometry in the gas phase (System II) shows an out-of-plane distortion of the pyrimidine ring, with a C_9-N_{10}-C_{10a}-N_1 dihedral angle of 72.9° (Figure 1B). The E_F in the gas phase (System II) estimated with this distorted geometry at the TD-CAM-B3LYP/def2-TZVP level is rather small with a value of only 0.81 eV. The distorted geometry is similar to the intersection structure obtained with N(5)-methylated LFOH using *ab initio* multiconfigurational quantum chemistry, in which the dihedral angle is ca. 85°.[33] Furthermore, the oscillator strength (*f*) under vacuum was calculated to be 0.001, a rather small value indicating negligible fluorescence. In contrast, the value in the protein was calculated to be 0.133, more than 100-fold enhancement compared to the case under vacuum. Therefore, our results support the assertion that the protein environment restraints the isoalloxazine ring to its planar fluorescent state, which blocks the CI-mediated internal conversion pathway and thus increases the fluorescence quantum yield.[33-34] Additionally, the results obtained with TD-DFT method are generally consistent with those obtained using the more computationally expensive state-of-the-art multireference method,[29, 33-34] demonstrating the informative nature of the TD-DFT approach.

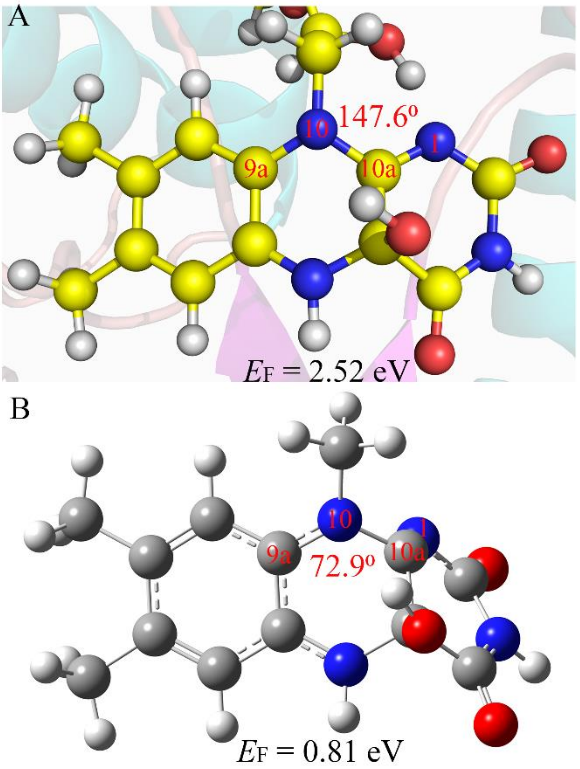

Figure 1. Comparison of chromophore (HFOH) structures in the protein environment (System I) and in the gas phase (System II). (A) QM(TD-CAM-B3LYP/6-31+G**)/MM optimized geometry of first excited state ^{1}HFOH* in the protein environment. (B) TD-CAM-B3LYP/6-31+G** optimized geometry of first excited state ^{1}HFOH* under vacuum. A key dihedral angle of C_{9a}-N_{10}-C_{10a}-N_1 that characterizes planarity of the isoalloxazine ring is shown in both cases, along with the energy difference between the S_0 state and S_1 state (E_F).

3.2 Fluorescence spectral properties of the planar ^{1}LFOH*. As noted by List et al.,[52] the electrostatic effect imposed by the protein can be determined by comparing the results obtained with the bare fluorophore in System III and the results obtained with the fluorophore embedded in the protein (System I). After examining the importance of geometry confinement exerted by the protein environment, we now turn to investigating the electronic emission properties of HFOH employing the bare fluorophore with the planar structure observed in the protein (System III). Notably, the fluorophore in these two cases adopts the same geometry, as obtained using the QM/MM method (refer to Figure 1A), to eliminate the interference of conformational effect. Similarly, the electrostatic effect of polar solvents can be obtained by comparing the results for the planar geometry of the bare chromophore in the gas phase and in different solvents.

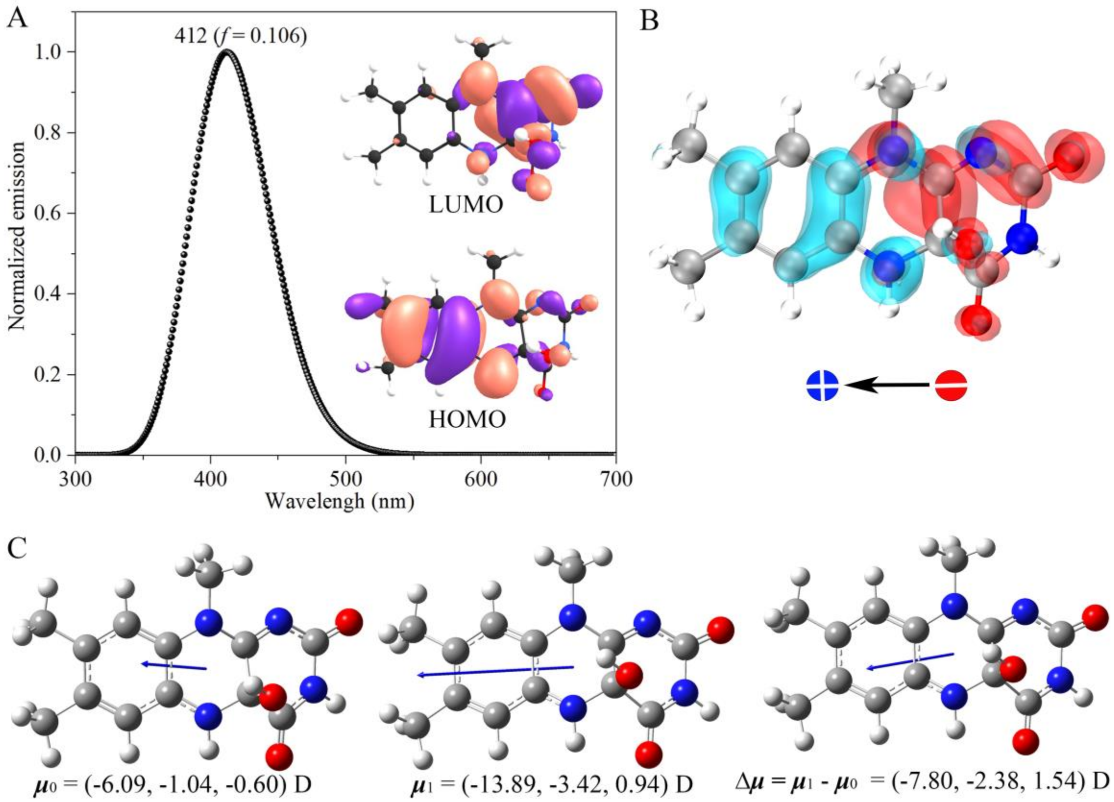

Figure 2. Fluorescence spectral properties of ^{1}LFOH* obtained with TD-CAM-B3LYP/def2-TZVP method in the gas phase using the planar geometry. (A) Normalized fluorescence spectra under vacuum, along with the related frontier orbitals. (B) Hole (blue) and electron (red) isosurfaces of $S_0 \rightarrow S_1$ transition of ^{1}LFOH*. The isosurface value is set to 0.002. (C) Permanent dipole moments of the ground S_0 ($\boldsymbol{\mu}_0$) and first excited S_1 ($\boldsymbol{\mu}_1$) states, and the difference dipole moment ($\Delta\boldsymbol{\mu}$).

The fluorescence spectral properties of HFOH were calculated using the simplified model molecule LFOH, with TD-CAM-B3LYP/def2-TZVP method consistent with above QM/MM calculations. The first excited state (S_1) is primarily (96.5%) represented by a one-electron promotion from the highest occupied molecular orbital (HOMO, π) to the lowest unoccupied molecular orbital (LUMO, π^*). The calculated vertical emission energy from the S_1 to S_0 state is 3.01 eV, corresponding to a fluorescence wavelength of 412 nm (Figure 2A). Notably, it is about 80 nm shorter than the emission maximum of ca. 490 nm observed in the protein environment.[30] With the planar conformation, the calculated oscillator strength (f) is 0.106, much stronger than the value of 0.001 estimated for the distorted conformation. Analysis of the frontier molecular orbitals shows the HOMO is delocalized over the isoalloxazine ring, while the LUMO is mainly concentrated on the pyrimidine ring (insets of Figure 2A). Accordingly, the right pyrimidine ring becomes more electron-rich, while the rest of the molecule becomes electron-deficient upon S_0 to S_1 promotion, which is verified by the hole and electron map (Figure 2B).[96] The calculated dipole moment of the S_0 state ($\boldsymbol{\mu}_0$) is 6.20 D, pointing approximately in the negative X direction (Figure 2C). For the S_1 state, the dipole moment ($\boldsymbol{\mu}_1$) is much larger with a magnitude of 14.33 D, pointing nearly in the same direction (Figure 2C). The large difference dipole moment ($\Delta\boldsymbol{\mu} = \boldsymbol{\mu}_1 - \boldsymbol{\mu}_0 = 8.30$ D) indicates that the S_1 state has a significant charge transfer (CT) character, which can be further confirmed from the hole and electron map shown in Figure 2B.

3.3 Electrostatic effect of polar solvents. Next, we seek to understand how the fluorescence spectrum of HFOH may be affected by electrostatic effect. First, we investigated the effect of solvent polarity, which can be used to detect the polarity of the environment surrounding the fluorophore. TD-DFT calculations were performed using the polarizable continuum model (PCM)[91-92] to account for the change in electronic properties due to solvent polarity. This approach has been commonly used to study the effect of the luciferase cavity on bioluminescence.[36, 97-98] To exclude conformational effect, the electrostatic effect calculations were studied with System III based on a fixed geometry, namely the planar QM/MM-optimized geometry shown in Figure 1A.

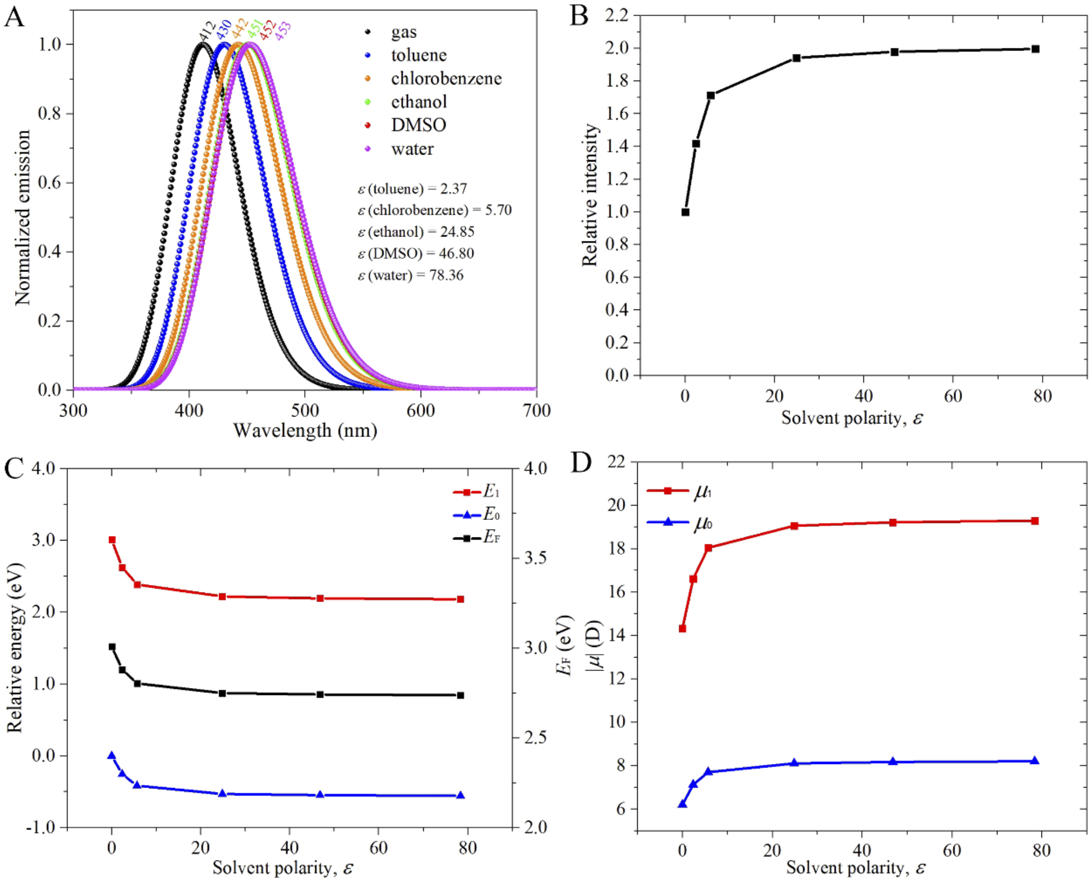

Figure 3. Electrostatic effect of solvent polarity on the fluorescence spectral properties of ^{1}LFOH*. (A) Normalized fluorescence spectra in implicit solvents with different dielectric constant (ε). (B) Dependence of fluorescence intensity on the solvent polarity. The intensities are normalized by the intensity under vacuum. (C) Dependence of the ground state energy (E_0), first excited energy (E_1), and vertical emission energy (E_F) on the solvent polarity. The energies of E_0 and E_1 are relative to the value of E_0 under vacuum. (D) Dependence of the magnitude of the dipole moment of ground state (μ_0) and first excited state (μ_1) on the solvent polarity.

Figure 3A shows the shift of the fluorescence spectrum under the influence of different polar solvents. Generally, the emission maximum λ_F is red-shifted to longer wavelengths as the solvent polarity increases. To be more specific, the dielectric effect can be divided into regimes of low ($\varepsilon < 25$) and high ($\varepsilon > 25$) polarity. In the low-polarity regime, the spectral shifting due to polarity change is significant. Conversely, in the high-polarity regime, the change in emission wavelength is much smaller or even negligible. Intriguingly, the variation trend is consistent with the one observed for the fluorophore in the firefly system,[36] indicating the generality of this spectral regulation rule by solvent polarity. Figure 3B shows the variation of spectral intensity upon the change of solvent polarity. The intensity increases as the solvent polarity increases with a stronger dependence in the low-polarity regime compared to the high-polarity regime (Figure 3B). The computed energies of the S_0 and S_1 states (E_0 and E_1, respectively) under different solvents (Figure 3C) show that: (1) polar solvents stabilize both S_0 and S_1 states; (2) the stabilization effect is stronger for solvents with larger dielectric constants (ε); (3) the stabilization effect is slightly stronger for the S_1 state than the S_0 state. Therefore, it is the different stabilization of the S_0 and S_1 states that leads to the observed red-shift in the emission spectrum with increasing solvent polarity. It is well-known that the electrostatic interaction directly correlates with the magnitude of the dipole moment, a larger dipole moment corresponding to a stronger stabilization. To understand the variation trend of E_0 and E_1, the dipole moments of the S_0 and S_1 states ($\boldsymbol{\mu_0}$ and $\boldsymbol{\mu_1}$, respectively) under different solvents were calculated. As shown in Figure 3D, both $\boldsymbol{\mu_1}$ and $\boldsymbol{\mu_0}$ increase with increasing ε, and $\boldsymbol{\mu_1}$ is always larger than $\boldsymbol{\mu_0}$. The increase of $\boldsymbol{\mu_1}$ and $\boldsymbol{\mu_0}$ results in the decrease of E_1 and E_0, respectively. Moreover, the larger value of $\boldsymbol{\mu_1}$ compared to $\boldsymbol{\mu_0}$ readily explains the stronger stabilization of the S_1 state compared to the S_0 state. Thus, the variation trend of E_1 and E_0 shown in Figure 3C can be well explained by the change of the dipole moments shown in Figure 3D, which accounts for the observed variation in the fluorescence spectrum with solvent polarity shown in Figure 3A.

3.4 Effect of OEEFs. It should be noted that the electric field around the fluorophore in the protein cavity is not uniform and quite different from the local electric field in a polar solvent. An approach to take into account the nonuniformity of the electrostatic environment is applying an oriented external electric field.[36] The insight obtained above with implicit solvent model shows how a homogeneous dielectric environment affects the fluorescence spectrum. However, investigating the effect of OEEFs is more useful for capturing the heterogeneous electrostatic effects and predicting how the change at a particular position (such as the mutation of a specific amino acid of the protein) may influence the spectrum.

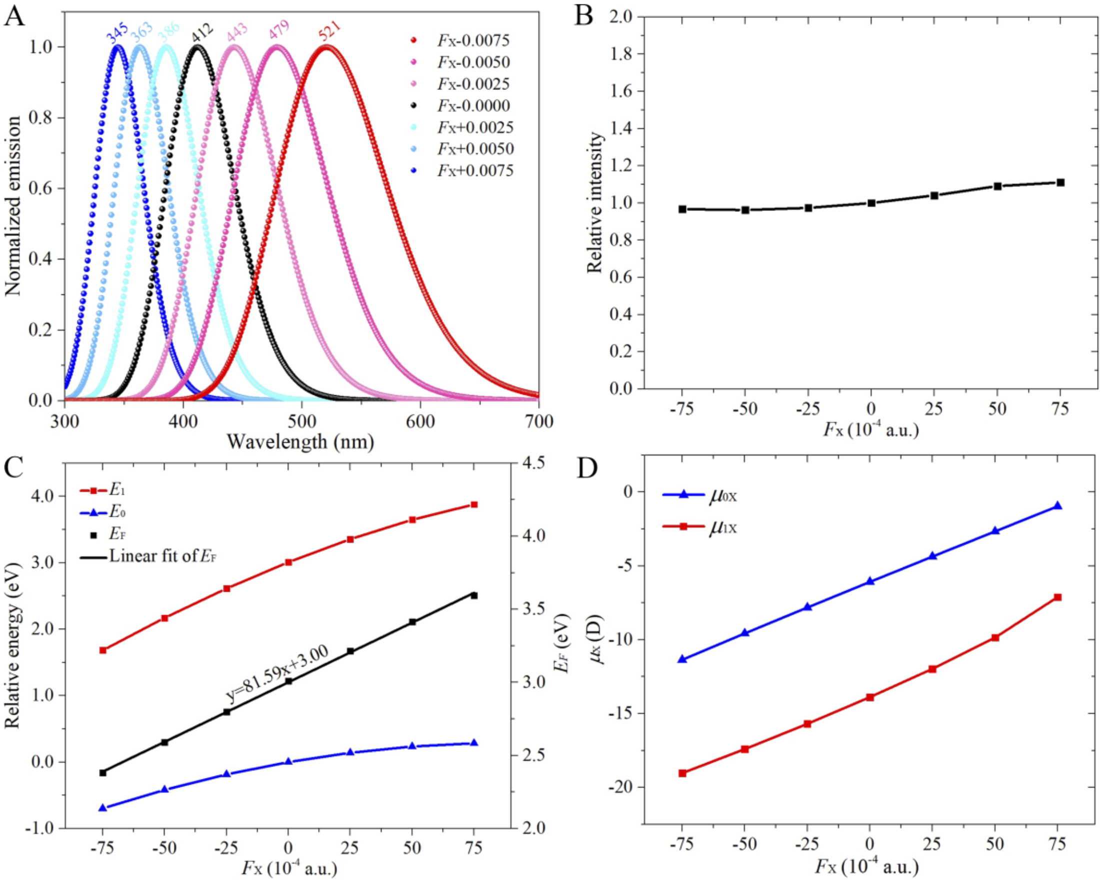

Figure 4. The effect of F_X on the fluorescence spectral properties of ^{1}LFOH*. (A) Normalized fluorescence spectra under different F_X. (B) Variation of fluorescence intensity as a function of F_X. The intensities are normalized by the intensity at zero field (F_X = 0.0000 a.u.). (C) Variation of the ground state energy (E_0), first excited energy (E_1), and vertical emission energy (E_F) as a function of F_X. The energies of E_0 and E_1 are relative to the value of E_0 at zero field. The black line represents the linear fit to the data of E_F. (D) Variation of the X component of the dipole moment of the ground state (μ_{0X}) and the first excited state (μ_{1X}) as a function of F_X.

The OEEFs were applied along three mutually perpendicular directions, as illustrated in **Scheme 2**. The fluorescence wavelength (λ_F) was found to be most sensitive to the OEEFs along the X axis (F_X), but much less sensitive to the fields along the Y and Z axes (refer to Figures S1-S4 and Figures S5-S8 for the effect of F_Y and F_Z, respectively). Applying a positive F_X field leads to a blueshift in fluorescence wavelength, while a negative F_X gives rise to a redshift (Figure 4A). The spectral shifting directly correlates with the field strength, stronger fields resulting in larger offsets. Specifically, a F_X field of -0.0075 a.u. reduces the vertical emission energy (E_F) by 0.63 eV from 3.01 eV to 2.38 eV, shifting λ_F from 412 nm to 521 nm. Contrary to above case of polar solvents, the fluorescence intensity was found to be insensitive to F_X (Figure 4B). For F_Y, positive fields result in blueshifts, while negative fields result in redshifts. The effect of F_Y is much smaller than that of F_X. Applying a negative field of F_Y = -0.0075 a.u. reduces E_F by only 0.20 eV from 3.01 eV to 2.81 eV, red-shifting λ_F by 29 nm from 412 nm to 441 nm. In contrast, positive F_Z fields redshift the wavelength while negative F_Z fields lead to blueshifts. The decrease of E_F induced by F_Z = 0.0075 a.u. is only 0.13 eV (from 3.01 eV to 2.88 eV), corresponding to an offset of only 9 nm for λ_F. Since there is a small difference between the TD-DFT/MM-optimized geometry in this study and the geometry previously obtained by some of us using the multi-reference method,[29] we also tested the effect of OEEFs using this geometry. The results are collectively shown in Figures S9-S11. Overall, the effects of OEEFs are totally consistent with the results discussed above, further validating the robustness of our results (refer to Note 1 in the SI).

To get insight into how the OEEFs affect the properties of the spectrum, we first analyzed the variation of E_0 and E_1 under F_X. As shown in Figure 4C, increasing the field strength raises the energy of both the S_0 and S_1 states, but the energy change differs between the two states. Conversely, decreasing the field strength leads to a decrease of both E_0 and E_1. Similar to the case of polar solvents, the S_1 state is more sensitive to the field than the S_0 state, and the change of E_1 is much larger than the change of E_0 for the same field strength. Intriguingly, the vertical emission energy ($E_F = E_1 - E_0$) responds linearly to the field strength of F_X, with a larger field leading to a larger E_F. The relationship between E_F and F_X can be fitted with a simple equation: $E_F = 81.59\ F_X + 3.00$. The linear and continuous dependence of E_F on the electric field indicates the feasibility of intentional and accurate color tuning through control of the local electric field, as well as the ability to detect electric field strength through the spectrum. In order to understand why S_1 state is more sensitive to the field, the values of both $\boldsymbol{\mu_0}$ and $\boldsymbol{\mu_1}$ under F_X were calculated. To facilitate subsequent discussions, the X component of $\boldsymbol{\mu_1}$ and $\boldsymbol{\mu_0}$ is denoted as μ_{1X} and μ_{0X}, respectively. As shown in Figure 4D, both μ_{1X} (red line) and μ_{0X} (blue line) are negative within the applied field strength (0.0075 a.u.). Additionally, the magnitude of μ_{1X} is always larger than μ_{0X}, and both μ_{0X} and μ_{1X} respond linearly to the field strength. Finally, the difference between μ_{1X} and μ_{0X} remains nearly unchanged. The negative value of the dipole moment indicates that a negative field stabilizes the dipole moment and lowers its energy, while a positive field has the opposite effect. The larger magnitude of μ_{1X} compared to μ_{0X} explains the greater field effect of F_X on the S_1 state than the S_0 state. The linear response of E_F to F_X, along with the consistent difference between μ_{1X} and μ_{0X}, demonstrate the dominating role of the first-order Stark effect within the field strength used in this study: $\Delta E_F = E_F - E_{F=0} = -\Delta\mu_{F=0} \times F$. The value (81.59 eV/a.u. = 7.62 D) of the slope of the linear fit in Figure 4C is close to the negative value (7.80 D) of the X component of the field-free difference dipole moment, further supporting this interpretation. Above analysis also applies to the cases of F_Y (refer to Figures S3) and F_Z (refer to Figures S7). Overall, the dipole moment analysis gives a well explanation of the effect of OEEFs (refer to Note 2 for a more quantitative discussion in SI), reminiscent of the case of the selectivity control of Diel-Alder reactions by OEEFs.[99-100]

Scheme 3. Three possible interaction modes of OEEFs.

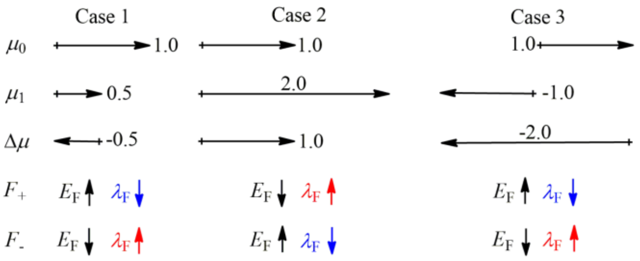

In order to give a quick prediction of the OEEF effect, we summarize three possible interaction modes of OEEFs in **Scheme 3**. For simplicity, the one-dimensional situation is considered. In actual situations, the direction of the difference dipole moment can be chosen to simplify the problem and maximize the effect of OEEFs. Assuming that the ground state dipole moment (μ_0) has a magnitude of 1.0 D, three different situations can be envisioned. In the first two cases, the excited state dipole moment (μ_1) is positive. In case 1, μ_1 is smaller than μ_0, while in case 2, μ_1 is larger than μ_0. In the last case, the direction of μ_1 is opposite to that of μ_0. Without loss of generality, the value of μ_1 can be assumed to be 0.5 D, 2.0 D and -1.0 D, in cases 1, 2 and 3, respectively. Consequently, the value of the difference dipole moment $\Delta\mu = \mu_1 - \mu_0$, can be obtained as -0.5 D, 1.0 D, and -2.0 D in cases 1, 2 and 3, respectively. When a positive field is applied, the field stabilizes the ground S_0 state due to the alignment of its dipole moment. Similarly, the positive field will lower the energy of the S_1 state in cases 1 and 2, but with different magnitudes due to their different dipole moments. In case 1, the stabilization effect on the S_1 state is weaker than the S_0 state. As a result, the emission energy E_F is increased, and the emission maximum λ_F is blue-shifted by the positive field. In case 2, the situation is reversed, and the stabilization effect on the S_1 state is stronger than the S_0 state. Consequently, E_F is decreased, and λ_F is red-shifted by the positive field. Notably, the situation of LFOH or HFOH discussed above is consistent with case 2. In case 3, a positive field destabilizes S_1 state due to its negative dipole moment. Thus, the energy gap between the S_0 state and S_1 state (E_F) is greatly enlarged due to the decrease of E_0 and the simultaneous increase of E_1. Accordingly, the wavelength will be largely blue-shifted by the positive field in case 3. A negative field leads to the exact opposite effect in all three cases. According to **Scheme 3**, the above analysis can be simplified by using difference dipole moment $\Delta\mu$, which can be obtained experimentally.[50, 101-102] *A field along the same direction as* $\Delta\mu$ *decreases* E_F *and redshifts the spectrum, whereas a field in the opposite direction increases* E_F *and blueshifts the spectrum.*

3.5 Correlation between the vertical emission energy and the LUMO-HOMO gap. Many previous studies have evaluated the spectral shift under internal or external electric field by correlating the vertical emission energy (E_F) values with the LUMO-HOMO gap.[54, 57-58, 60, 103] As shown in Figure S13, increasing solvent polarity raises the HOMO energy but lowers the LUMO energy, thus decreasing the LUMO-HOMO gap. The variation of HOMO and LUMO energies and the LUMO-HOMO gap as a function of F_X was shown in Figure S14. Under F_X, increasing the field strength lowers HOMO energy yet raises LUMO energy, therefore broadening the gap between them. Inverse trends are observed when decreasing F_X. Interestingly, a linear relationship is found between the LUMO-HOMO gap and E_F in both cases (Figure 5). A larger E_F corresponds to a larger HOMO-LUMO gap, validating the use of the HOMO-LUMO gap variation to illustrate the change of E_F. However, it is noteworthy that the parameters used to fit the data are different between the two cases shown in Figure 5A and 5B. The line in the case of F_X (Figure 5B) has a steeper slope than that in polar solvents (Figure 5A), indicating different spectral tuning mechanisms. Besides, it is worth noting that the first excited S_1 state still corresponds to the HOMO → LUMO transition under polar solvents (Table S3) and within the electric field strength explored (Table S4), yet the energy order of frontier orbitals may change in stronger fields due to their different response characteristics, in which case the linear relationship shown in Figure 5B may no longer be valid. A more direct and precise understanding of the change in E_F can be obtained by examining the changes in S_0 and S_1 energies, as shown in Figure 3C and 4C. Additionally, since the interaction with electrostatic environments, such as polar solvents or OEEFs, directly correlates with their dipole moments, the energy changes of the S_0 and S_1 states can be easily predicted qualitatively or even quantitatively based on their dipole moments.

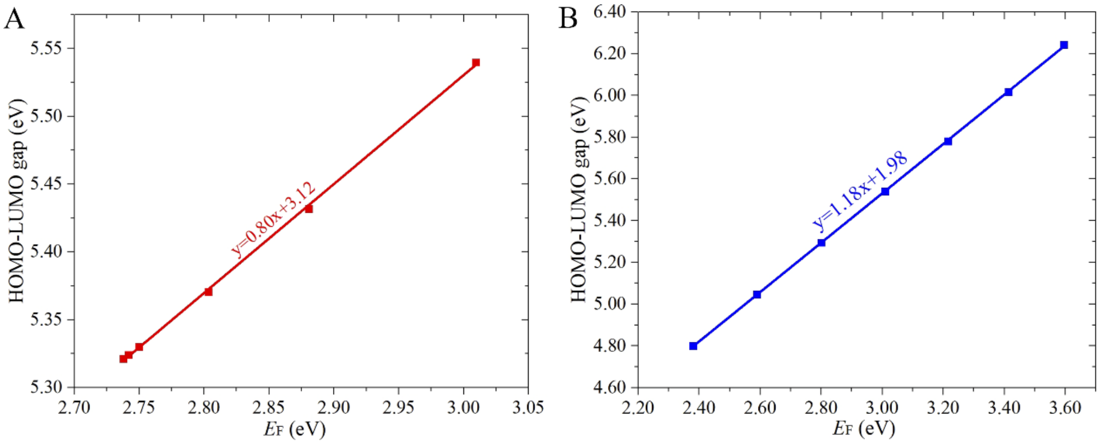

Figure 5. Correlation of the vertical emission energy (E_F) and the LUMO-HOMO energy gap in the case of polar solvents (A) and oriented external electric field F_X (B).

3.6 How the intensity is affected by electrostatic environments. The intensity of fluorescence is another important property that may be significantly affected by electrostatic environments. As shown in Figure 3B, the intensity changes greatly with different solvent polarities, especially in the low-polarity regime. In contrast, only negligible changes are observed when applying OEEFs (refer to Figure 4B, Figure S2, and Figure S6). Specifically, the emission maximum is redshifted from 412 nm in vacuum to 453 nm in water, accompanied with a substantial intensity enhancement of 99% (0.211 vs 0.106 in water and in vacuum, respectively). On the contrary, when F_X = -0.0050 a.u. is applied, although the emission maximum has been redshifted to 479 nm the intensity only decreases by 4% (0.102 vs 0.106 under F_X = -0.0050 a.u. and F_X = 0.0000 a.u., respectively). Overall, these contrasting observations indicate that the intensity tuning mechanisms induced by polar solvents and OEEFs are fundamentally different.

The fluorescence intensity can be characterized by the dimensionless parameter f (oscillator strength), which correlates with the emission energy E_F and the transition dipole moment strength $|\boldsymbol{\mu}_\mathrm{T}|$, as shown in Equation 1:

$$f = \mathrm{A}E_\mathrm{F} \times |\boldsymbol{\mu}_\mathrm{T}|^2, \tag{1}$$

where A is a constant.[104] To simplify the expression of Eq. 1 and facilitate analysis, three new variables are defined to describe the variation of the three variables in Eq. 1:

$$R_\mathrm{F} = f/f_0, \tag{2}$$

$$R_\mathrm{E} = E_\mathrm{F}/E_{\mathrm{F}0}, \tag{3}$$

$$R_D = |\boldsymbol{\mu}_\mathrm{T}|^2/|\boldsymbol{\mu}_{\mathrm{T}0}|^2, \tag{4}$$

where the subscripts with 0 represent the parameters of the reference state. For polar solvents, the reference state is chosen as the state under vacuum, whereas the field-free state (F_X = 0.0000 a.u.) is selected as the reference state for F_X. Accordingly, Eq. 1 can be transformed to below equation:

$$R_\mathrm{F} = R_\mathrm{E} \times R_\mathrm{D}. \tag{5}$$

Expectedly, a deep understanding of how the intensity is affected can be obtained through a dependency analysis among the three predefined variables, R_F, R_E and R_D. For polar solvents (Figure 6A), the variation of R_F is strongly and positively correlated with the variation of R_D, while it is only weakly and negatively correlated with R_E. Besides, it is notable that polar solvents induce a strong enhancement of R_D (or transition dipole moment, refer to Figure S15) yet a slight decrease of R_E (or vertical emission energy, E_F). Therefore, the intensity change in polar solvents mainly comes from the change of the transition dipole moment. In the case of F_X (Figure 6B), R_F is positively correlated with R_E and negatively correlated with R_D, and the effects of R_E and R_D offset each other, resulting in a negligible change of R_F. Indeed, scrutiny of the transition dipole moment shows that R_D is increased by negative F_X fields yet decreased by positive F_X fields (refer to Figure S16), which cancels out the variation of R_E. Notably, the variation of the transition dipole moment (or R_D) is much smaller under F_X compared to polar solvents. In summary, the intensity enhancement in polar solvents mainly comes from the increase of the transition dipole moment, while the slight variation of intensity under F_X originates from the mutual cancellation of the change of the vertical emission energy and the change of the transition dipole moment.

3.7 Electrostatic effect of the protein environment on the fluorescence spectrum. After elucidating the electrostatic effect of polar solvents and OEEFs, we now seek to gain insight into how the protein environment affects the fluorescence spectrum of ^{1}HFOH*. A direct comparison between System I and System III shows that λ_F is redshifted from 412 nm to 493 nm by the electrostatic effect of the protein environment. As shown above, either increasing solvent polarity or applying an OEEF in the negative F_X direction can lead to a significant redshift of λ_F. In the implicit solvent model of chlorobenzene (ε = 5.70) that is commonly used to mimic the protein electrostatic environment,[105-108] the calculated λ_F is redshifted to 442 nm (Figure 3A), yet it is still 48 nm shorter than the 490 nm observed experimentally in the protein. Interestingly, the redshift of the emission wavelength in the protein can be rationalized by the presence of an internal electric field (IEF) of F_X = -0.0057 a.u. = -29.3 MV/cm (refer to Figure S17). Notably, the IEF within the protein cavity is not uniform, but rather varies across the isoalloxazine ring of the fluorophore. Therefore, the estimated electric field can be viewed as an effective field representing the spatially heterogeneous IEF.

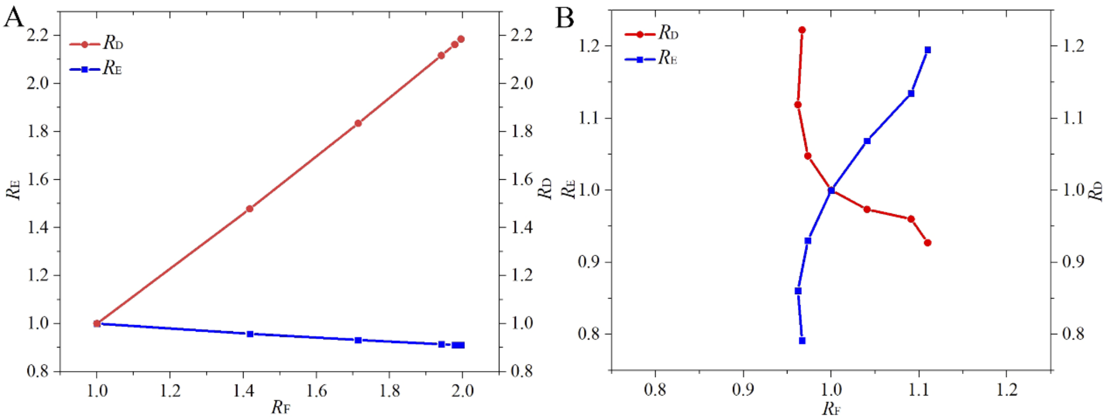

Figure 6. (A) Dependency analysis of R_F, R_E and R_D in the case of polar solvents. The parameters are normalized by the values in vacuum. (B) Dependency analysis of R_F, R_E and R_D in the case of F_X fields. The parameters are normalized by the field-free values. Definitions of R_F, R_E and R_D can be found in the main text.

The key charged residues that contribute to the IEF along the long axis of the fluorophore (X-axis), in both positive and negative directions, are shown in Figure 7. Negatively charged residues located on the left side, such as Glu175, Glu200, and Asp314, as well as positively charged residues on the right side, like His45, Arg107, Lys112, Lys286, and Arg85 of chain B, produce a negative F_X field. Conversely, the positively charged residues on the left side, including Lys201 and Arg290, and the negatively charged residues on the right side, such as Glu43, Asp111, Asp113, and Glu88 of the chain B, generate a positive F_X field. Therefore, mutations at these positions are predicted to lead to considerable changes in the emission wavelength (λ_F).[109] Based on this understanding, a rational design of new variants of bacterial luciferase becomes possible. For example, to obtain fluorescence with a longer wavelength, one would need to introduce a more negative F_X field, which could be achieved by engineering either positively charged residues on the right side or negatively charged residues on the left side of the fluorophore through site-directed mutagenesis.

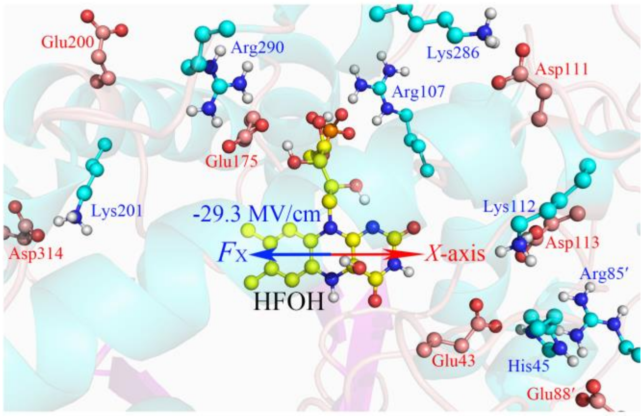

Figure 7. Key charged residues near the fluorophore. Positively charged residues are labelled in blue, while negatively charged residues are labelled in red. Residues in chain B are labelled with a prime. Notably, the internal electric field at the active site possesses a negative X component.

Conclusions.

In summary, the fluorescence spectral tuning mechanism of bacterial luciferase has been systematically investigated from a theoretical perspective. In line with previous studies, the geometry confinement by the indirect steric effect of the protein surroundings is key to its fluorescence efficiency, as it maintains the chromophore in a planar conformation and blocks excited state deactivation via a CI-mediated internal conversion. On the other hand, the fine-tuning of the fluorescence spectroscopic properties, including emission wavelength and intensity, can be achieved through electrostatic effect, such as embedding the chromophore in a homogeneous dielectric environment or applying OEEFs. Increasing solvent polarity leads to a red-shift of the fluorescence emission maximum λ_F and an increase in intensity. Furthermore, the effect of solvent polarity can be divided into two regimes, a low-polarity regime ($\varepsilon < 25$) and a high polarity regime ($\varepsilon > 25$). Both emission wavelength and intensity are more sensitive in the low-polarity regime than in the high-polarity regime. A red-shift in wavelength can also be achieved by applying a negative F_X field along the long axis of the isoalloxazine ring. The emission maxima can be redshifted by more than 100 nm with a moderate filed strength of 0.0075 a.u. (38.6 MV/cm). Intriguingly, the redshift of the wavelength under F_X is accompanied by a negligible change of intensity, in sharp contrast with the case of solvent polarity. OEEFs provide a more flexible method to control the fluorescence wavelength, a positive field blue-shifting the emission wavelength.

The spectral red-shifting observed in homogeneous polar solvents can be well explained by the larger dipole moment of the S_1 state compared to the S_0 state. A larger dipole moment of the S_1 state leads to a stronger stabilization effect by the polar environment, which decreases the energy difference between the S_1 and S_0 states, thus causing a redshift of the emission wavelength. In the implicit solvent model, the environment is homogenous in any direction, and the interaction exerted on the chromophore correlates with its total dipole moment. In contrast, the effect of OEEFs is directional and correlates with the component of the difference dipole moment along the specific direction of the applied field. In the current case of LFOH or HFOH, the charge redistribution upon S_0 to S_1 promotion mainly occurs along the long axis of the isoalloxazine ring (X-axis). Accordingly, the spectrum is most sensitive to F_X and much less sensitive to F_Y and F_Z. Qualitatively, applying a field along the direction of the field-free difference dipole moment decreases the emission energy E_F and thus leads to the redshift of the emission maximum λ_F, while an opposite field increases E_F and blueshifts λ_F. Within the field strength applied in this study (0.0075 a.u.), the effect of OEEFs obeys the first-order Stark effect. The emission energy E_F responses linearly to the electric field, and its variation is proportional to the component of the field-free difference dipole moment along the field direction. Therefore, a field along the direction of the difference dipole moment is most efficient for spectral modulation. The linear and continuous dependence indicates the feasibility of intentional and accurate color tuning through control of the local electric field. As for intensity, the substantial enhancement in polar solvents comes from the increase of the transition dipole moment. Notably, in the case of F_X, E_F experiences a larger variation compared to the case of polar solvents, which in principle would lead to a considerable change in intensity. However, the variation of the transition dipole moment offsets the change induced by E_F, resulting in only a slight variation of intensity under F_X.

Last but not least, the significant redshift of the emission wavelength in the protein environment indicates the presence of a non-negligible IEF in the negative X direction. This IEF mainly originates from the charged amino acid residues surrounding the fluorophore, and mutation at these positions may result in considerable changes in the fluorescence emission maximum. The spectral tuning mechanisms discovered in this study are helpful to elucidating the key amino acid residues and the role of point mutations, as well as to the rational design of improved fluorescent proteins.

ASSOCIATED CONTENT

Supporting Information: Figures S1-S17, Table S1-S26, Notes 1 and 2, and the cartesian coordinates of the optimized geometries (PDF)

AUTHOR INFORMATION

Corresponding Author

*Zhanfeng Wang, zfwang@bnu.edu.cn

ORCID

Yanling Luo: orcid.org/0009-0005-2443-1934

Zhanfeng Wang: orcid.org/0000-0001-6722-2298

Notes

The authors declare no competing financial interest.

ACKNOWLEDGMENT

This work was supported by grants from the National Natural Science Foundation of China (No. 22203007 to Z. W., Nos. 22373010 and 21973005 to Y. L.), and the Startup Funding from Beijing Normal University (No. 310432104 to Z.W.). The authors thank support from the Interdisciplinary Intelligence Super Computer Center of Beijing Normal University at Zhuhai.

ABBREVIATIONS

TD-DFT, time-dependent density functional theory; QM/MM, quantum mechanics/molecular mechanics; MD, molecular dynamics; OEEF, oriented external electric field; IEF, internal electric field; FMN, flavin mononucleotide; HFOOH, 4a-hydroperoxy-5-hydro-FMN; HFOOCH(OH)R, 4a-peroxyhemiacetal-5-hydro-FMN; HFOH, 4a-hydroxy-5-hydro-FMN; LFOH, 4a-hydroxy-5-hydro-lumiflavin; GFP, green fluorescent protein; GAFF, general amber force field; PCM, polarizable continuum mode; CI, conical intersection; HOMO, highest occupied molecular orbital; LUMO, lowest unoccupied molecular orbital; CT, charge transfer; E_F, vertical emission energy; λ_F fluorescence wavelength.

REFERENCES

1. Vacher, M.; Galván, I. F.; Ding, B. W.; Schramm, S.; Berraud-Pache, R.; Naumov, P.; Ferré, N.; Liu, Y. J.; Navizet, I.; Roca-Sanjuán, D.; Baader, W. J.; Lindh, R., Chemi- and Bioluminescence of Cyclic Peroxides. *Chem Rev* **2018,** *118* (15), 6927-6974.
2. Syed, A. J.; Anderson, J. C., Applications of bioluminescence in biotechnology and beyond. *Chem Soc Rev* **2021,** *50* (9), 5668-5705.
3. Liu, Y. J., Understanding the complete bioluminescence cycle from a multiscale computational perspective: A review. *J Photoch Photobio C* **2022,** *52*.
4. Letendre, F.; Twardowski, M.; Blackburn, A.; Poulin, C.; Latz, M. I., A review of mechanically stimulated bioluminescence of marine plankton and its applications. *Front Mar Sci* **2024,** *10*, 1299602.
5. Schramm, S.; Weiss, D., Bioluminescence - The Vibrant Glow of Nature and its Chemical Mechanisms. *Chembiochem* **2024,** *25* (9).
6. Li, Y.; He, X.; Zhu, W.; Li, H.; Wang, W., Bacterial bioluminescence assay for bioanalysis and bioimaging. *Analytical and Bioanalytical Chemistry* **2022,** *414* (1), 75-83.
7. Iwano, S.; Sugiyama, M.; Hama, H.; Watakabe, A.; Hasegawa, N.; Kuchimaru, T.; Tanaka, K. Z.; Takahashi, M.; Ishida, Y.; Hata, J.; Shimozono, S.; Namiki, K.; Fukano, T.; Kiyama, M.; Okano, H.; Kizaka-Kondoh, S.; McHugh, T. J.; Yamamori, T.; Hioki, H.; Maki, S.; Miyawaki, A., Single-cell bioluminescence imaging of deep tissue in freely moving animals. *Science* **2018,** *359* (6378), 935-939.
8. Contag, C. H.; Bachmann, M. H., Advances in vivo bioluminescence imaging of gene expression. *Annu Rev Biomed Eng* **2002,** *4*, 235-260.
9. Momota, H.; Holland, E. C., Bioluminescence technology for imaging cell proliferation. *Curr Opin Biotech* **2005,** *16* (6), 681-686.
10. Axelrod, T.; Eltzov, E.; Marks, R. S., Bioluminescent bioreporter pad biosensor for monitoring water toxicity. *Talanta* **2016,** *149*, 290-297.
11. Steinberg, S. M.; Poziomek, E. J.; Engelmann, W. H.; Rogers, K. R., A Review of Environmental Applications of Bioluminescence Measurements. *Chemosphere* **1995,** *30* (11), 2155-2197.
12. Alloush, H. M.; Lewis, R. J.; Salisbury, V. C., Bacterial bioluminescent biosensors: Applications in food and environmental monitoring. *Anal Lett* **2006,** *39* (8), 1517-1526.
13. Fernández-Piñas, F.; Rodea-Palomares, I.; Leganés, F.; González-Pleiter, M.; Muñoz-Martín, M. A., Evaluation of the Ecotoxicity of Pollutants with Bioluminescent Microorganisms Evaluation of the Ecotoxicity of Pollutants with Bioluminescent Microorganisms. *Adv Biochem Eng Biot* **2014,** *145*, 65-135.
14. Ran, C. Z.; Pu, K. Y., Molecularly generated light and its biomedical applications. *Angew Chem Int Edit* **2024,** *63* (6), e202314468.
15. Ai, H. W.; Olenych, S. G.; Wong, P.; Davidson, M. W.; Campbell, R. E., Hue-shifted monomeric variants of *Clavularia* cyan fluorescent protein: identification of the molecular determinants of color and applications in fluorescence imaging. *Bmc Biol* **2008,** *6*, 13.
16. Mezzanotte, L.; van 't Root, M.; Karatas, H.; Goun, E. A.; Lowik, C. W. G. M., Molecular Bioluminescence Imaging: New Tools and Applications. *Trends Biotechnol* **2017,** *35* (7), 640-652.

17. Maric, T.; Mikhaylov, G.; Khodakivskyi, P.; Bazhin, A.; Sinisi, R.; Bonhoure, N.; Yevtodiyenko, A.; Jones, A.; Muhunthan, V.; Abdelhady, G.; Shackelford, D.; Goun, E., Bioluminescent-based imaging and quantification of glucose uptake in vivo. *Nat Methods* **2019,** *16* (6), 526-532.

18. Khakhar, A.; Starker, C. G.; Chamness, J. C.; Lee, N.; Stokke, S.; Wang, C.; Swanson, R.; Rizvi, F.; Imaizumi, T.; Voytas, D. F., Building customizable auto-luminescent luciferase-based reporters in plants. *Elife* **2020,** *9,* e52786.

19. Carrasco-López, C.; Lui, N. M.; Schramm, S.; Naumov, P., The elusive relationship between structure and colour emission in beetle luciferases. *Nat Rev Chem* **2021,** *5* (1), 4-20.

20. Hou, C.; Liu, Y.-J.; Ferre, N.; Fang, W.-H., Understanding Bacterial Bioluminescence: A Theoretical Study of the Entire Process, from Reduced Flavin to Light Emission. *Chemistry-a European Journal* **2014,** *20* (26), 7979-7986.

21. Lee, J.; Mueller, F.; Visser, A. J. W. G., The Sensitized Bioluminescence Mechanism of Bacterial Luciferase. *Photochemistry and Photobiology* **2019,** *95* (3), 679-704.

22. Hastings, J. W.; Gibson, Q. H., Intermediates in the Bioluminescent Oxidation of Reduced Flavin Mononucleotide. *Journal of Biological Chemistry* **1963,** *238* (7), 2537-2554.

23. Vervoort, J.; Muller, F.; Okane, D. J.; Lee, J.; Bacher, A., Bacterial luciferase: a carbon-13, nitrogen-15, and phosphorus-31 nuclear magnetic resonance investigation. *Biochemistry* **1986,** *25* (24), 8067-8075.

24. Tu, S. C., Isolation and properties of bacterial luciferase intermediates containing different oxygenated flavins. *Journal of Biological Chemistry* **1982,** *257* (7), 3719-3725.

25. Wada, N.; Sugimoto, T.; Watanabe, H.; Tu, S. C., Computational analysis of the oxygen addition at the C_{4a} site of reduced flavin in the bacterial luciferase bioluminescence reaction. *Photochemistry and Photobiology* **1999,** *70* (1), 116-122.

26. Hastings, J. W.; Balny, C.; Lepeuch, C.; Douzou, P., Spectral properties of an oxygenated luciferase—flavin intermediate isolated by low-temperature chromatography. *P Natl Acad Sci USA* **1973,** *70* (12), 3468-3472.

27. Tu, S. C., Isolation and properties of bacterial luciferase-oxygenated flavin intermediate complexed with long-chain alcohols. *Biochemistry* **1979,** *18* (26), 5940-5945.

28. Macheroux, P.; Ghisla, S.; Hastings, J. W., Spectral detection of an intermediate preceding the excited state in the bacterial luciferase reaction. *Biochemistry* **1993,** *32* (51), 14183-14186.

29. Luo, Y.; Liu, Y.-J., Bioluminophore and Flavin Mononucleotide Fluorescence Quenching of Bacterial Bioluminescence-A Theoretical Study. *Chemistry-a European Journal* **2016,** *22* (45), 16243-16249.

30. Kurfurst, M.; Ghisla, S.; Hastings, J. W., Characterization and postulated structure of the primary emitter in the bacterial luciferase reaction. *P Natl Acad Sci USA* **1984,** *81* (10), 2990-2994.

31. Lei, B. F.; Ding, Q. Z.; Tu, S. C., Identity of the emitter in the bacterial luciferase luminescence reaction: Binding and fluorescence quantum yield studies of 5-decyl-4a-hydroxy-4a,5-dihydroriboflavin-5′-phosphate as a model. *Biochemistry* **2004,** *43* (50), 15975-15982.

32. Ghisla, S.; Massey, V.; Lhoste, J. M.; Mayhew, S. G., Fluorescence and optical characteristics of reduced flavines and flavoproteins. *Biochemistry* **1974,** *13* (3), 589-597.

33. Gozem, S.; Mirzakulova, E.; Schapiro, I.; Melaccio, F.; Glusac, K. D.; Olivucci, M., A Conical Intersection Controls the Deactivation of the Bacterial Luciferase Fluorophore. *Angew Chem Int Edit* **2014,** *53* (37), 9870-9875.

34. Giuliani, G.; Melaccio, F.; Gozem, S.; Cappelli, A.; Olivucci, M., QM/MM Investigation of the Spectroscopic Properties of the Fluorophore of Bacterial Luciferase. *J Chem Theory Comput* **2021,** *17* (2), 605-613.

35. Fried, S. D.; Bagchi, S.; Boxer, S. G., Extreme electric fields power catalysis in the active site of ketosteroid isomerase. *Science* **2014,** *346* (6216), 1510-1514.

36. Al-Handawi, M. B.; Polavaram, S.; Kurlevskaya, A.; Commins, P.; Schramm, S.; Carrasco-Lopez, C.; Lui, N. M.; Solntsev, K. M.; Laptenok, S. P.; Navizet, I.; Naumov, P., Spectrochemistry of Firefly Bioluminescence. *Chem Rev* **2022,** *122* (16), 13207-13234.

37. Diao, W.; Yan, S.; Farrell, J. D.; Wang, B.; Ye, F.; Wang, Z., Preorganized Internal Electric Field Powers Catalysis in the Active Site of Uracil-DNA Glycosylase. *Acs Catal* **2022,** *12* (20), 12488-12499.

38. Wang, Z.; Wang, B.; Diao, W.; Wu, P.; Li, J.; Fu, Y.; Guo, Z.; Cao, Z.; Shaik, S., How the Conformational Movement of the Substrate Drives the Regioselective C-N Bond Formation in P450 TleB: Insights from Molecular Dynamics Simulations and Quantum Mechanical/ Molecular Mechanical Calculations. *J Am Chem Soc* **2023,** *145* (13), 7252-7267.

39. Diao, W.; Farrell, J. D.; Wang, B.; Ye, F.; Wang, Z., Preorganized Internal Electric Field Promotes a Double-Displacement Mechanism for the Adenine Excision Reaction by Adenine DNA Glycosylase. *J Phys Chem B* **2023,** *127* (40), 8551-8564.

40. Dubey, K. D.; Stuyver, T.; Shaik, S., Local Electric Fields: From Enzyme Catalysis to Synthetic Catalyst Design. *J Phys Chem B* **2022,** *126* (49), 10285-10294.

41. Warshel, A., Energetics of Enzyme Catalysis. *P Natl Acad Sci USA* **1978,** *75* (11), 5250-5254.

42. Warshel, A.; Sharma, P. K.; Kato, M.; Xiang, Y.; Liu, H. B.; Olsson, M. H. M., Electrostatic basis for enzyme catalysis. *Chem Rev* **2006,** *106* (8), 3210-3235.

43. Fried, S. D.; Boxer, S. G., Electric Fields and Enzyme Catalysis. *Annu Rev Biochem* **2017,** *86,* 387-415.

44. Welborn, V. V.; Pestana, L. R.; Head-Gordon, T., Computational optimization of electric fields for better catalysis design. *Nat Catal* **2018,** *1* (9), 649-655.

45. Léonard, N. G.; Dhaoui, R.; Chantarojsiri, T.; Yang, J. Y., Electric Fields in Catalysis: From Enzymes to Molecular Catalysts. *Acs Catal* **2021,** *11* (17), 10923-10932.

46. Wang, Z. F.; Shaik, S.; Wang, B. J., Conformational Motion of Ferredoxin Enables Efficient Electron Transfer to Heme in the Full-Length P450. *J Am Chem Soc* **2021,** *143* (2), 1005-1016.

47. de Visser, S. P.; Mukherjee, G.; Ali, H. S.; Sastri, C. V., Local Charge Distributions, Electric Dipole Moments, and Local Electric Fields Influence Reactivity Patterns and Guide Regioselectivities in α-Ketoglutarate-Dependent Non-heme Iron Dioxygenases. *Accounts Chem Res* **2022,** *55* (1), 65-74.

48. Siddiqui, S. A.; Stuyver, T.; Shaik, S.; Dubey, K. D., Designed Local Electric Fields-Promising Tools for Enzyme Engineering. *Jacs Au* **2023,** *3* (12), 3259-3269.

49. Zheng, C.; Ji, Z.; Mathews, I. I.; Boxer, S. G., Enhanced active-site electric field accelerates enzyme catalysis. *Nat Chem* **2023,** *15* (12), 1715-1721.

50. Drobizhev, M.; Callis, P. R.; Nifosi, R.; Wicks, G.; Stoltzfus, C.; Barnett, L.; Hughes, T. E.; Sullivan, P.; Rebane, A., Long- and Short-Range Electrostatic Fields in GFP Mutants: Implications for Spectral Tuning. *Scientific Reports* **2015,** *5,* 13223.

51. Beerepoot, M. T. P.; Steindal, A. H.; Kongsted, J.; Brandsdal, B. O.; Frediani, L.; Ruud, K.; Olsen, J. M. H., A polarizable embedding DFT study of one-photon absorption in fluorescent proteins. *Phys Chem Chem Phys* **2013,** *15* (13), 4735-4743.

52. List, N. H.; Olsen, J. M. H.; Jensen, H. J. A.; Steindal, A. H.; Kongsted, J., Molecular-Level Insight into the Spectral Tuning Mechanism of the DsRed Chromophore. *Journal of Physical Chemistry Letters* **2012,** *3* (23), 3513-3521.

53. Kaila, V. R. I.; Send, R.; Sundholm, D., Electrostatic spectral tuning mechanism of the green fluorescent protein. *Phys Chem Chem Phys* **2013,** *15* (13), 4491-4495.

54. Topol, I.; Collins, J.; Savitsky, A.; Nemukhin, A., Computational strategy for tuning spectral properties of red fluorescent proteins. *Biophysical Chemistry* **2011,** *158* (2-3), 91-95.

55. Hirano, T.; Hasumi, Y.; Ohtsuka, K.; Maki, S.; Niwa, H.; Yamaji, M.; Hashizume, D., Spectroscopic Studies of the Light-Color

Modulation Mechanism of Firefly (Beetle) Bioluminescence. *J Am Chem Soc* **2009,** *131* (6), 2385-2396.

56. Nakatani, N.; Hasegawa, J.-y.; Nakatsuji, H., Red light in chemiluminescence and yellow-green light in bioluminescence: Color-tuning mechanism of firefly, *Photinus pyralis*, studied by the symmetry-adapted cluster-configuration interaction method. *J Am Chem Soc* **2007,** *129* (28), 8756-8765.

57. Cai, D. J.; Marques, M. A. L.; Nogueira, F., Accurate Color Tuning of Firefly Chromophore by Modulation of Local Polarization Electrostatic Fields. *J Phys Chem B* **2011,** *115* (2), 329-332.

58. Cai, D. J.; Marques, M. A. L.; Nogueira, F., Full Color Modulation of Firefly Luciferase through Engineering with Unified Stark Effect. *J Phys Chem B* **2013,** *117* (44), 13725-13730.

59. da Silva, L. P.; da Silva, J. C. G. E., Chemiexcitation Induced Proton Transfer: Enolate Oxyluciferin as the Firefly Bioluminophore. *J Phys Chem B* **2015,** *119* (6), 2140-2148.

60. Zhou, J. G.; Williams, Q. L.; Walters, W.; Deng, Z. Y., How Does the Local Electrostatic Field Influence Emitted Wavelengths and Bioluminescent Intensities of Modified Heteroaromatic Luciferins? *J Phys Chem B* **2015,** *119* (33), 10399-10405.

61. Campbell, Z. T.; Weichsel, A.; Montfort, W. R.; Baldwin, T. O., Crystal Structure of the Bacterial Luciferase/Flavin Complex Provides Insight into the Function of the β Subunit. *Biochemistry* **2009,** *48* (26), 6085-6094.

62. Waterhouse, A.; Bertoni, M.; Bienert, S.; Studer, G.; Tauriello, G.; Gumienny, R.; Heer, F. T.; de Beer, T. A. P.; Rempfer, C.; Bordoli, L.; Lepore, R.; Schwede, T., SWISS-MODEL: homology modelling of protein structures and complexes. *Nucleic Acids Res* **2018,** *46* (W1), W296-W303.

63. Dolinsky, T. J.; Nielsen, J. E.; McCammon, J. A.; Baker, N. A., PDB2PQR: an automated pipeline for the setup of Poisson-Boltzmann electrostatics calculations. *Nucleic Acids Res* **2004,** *32*, W665-W667.

64. Dolinsky, T. J.; Czodrowski, P.; Li, H.; Nielsen, J. E.; Jensen, J. H.; Klebe, G.; Baker, N. A., PDB2PQR: expanding and upgrading automated preparation of biomolecular structures for molecular simulations. *Nucleic Acids Res* **2007,** *35*, W522-W525.

65. Unni, S.; Huang, Y.; Hanson, R. M.; Tobias, M.; Krishnan, S.; Li, W. W.; Nielsen, J. E.; Baker, N. A., Web Servers and Services for Electrostatics Calculations with APBS and PDB2PQR. *J Comput Chem* **2011,** *32* (7), 1488-1491.

66. Tian, C.; Kasavajhala, K.; Belfon, K. A. A.; Raguette, L.; Huang, H.; Migues, A. N.; Bickel, J.; Wang, Y. Z.; Pincay, J.; Wu, Q.; Simmerling, C., ff19SB: Amino-Acid-Specific Protein Backbone Parameters Trained against Quantum Mechanics Energy Surfaces in Solution. *J Chem Theory Comput* **2020,** *16* (1), 528-552.

67. Wang, J. M.; Wolf, R. M.; Caldwell, J. W.; Kollman, P. A.; Case, D. A., Development and testing of a general amber force field. *J Comput Chem* **2004,** *25* (9), 1157-1174.

68. Cieplak, P.; Cornell, W. D.; Bayly, C.; Kollman, P. A., Application of the multimolecule and multiconformational RESP methodology to biopolymers: Charge derivation for DNA, RNA, and proteins. *J Comput Chem* **1995,** *16* (11), 1357-1377.

69. Frisch, M. J.; Trucks, G. W.; Schlegel, H. B.; Scuseria, G. E.; Robb, M. A.; Cheeseman, J. R.; Scalmani, G.; Barone, V.; Petersson, G. A.; Nakatsuji, H.; Li, X.; Caricato, M.; Marenich, A. V.; Bloino, J.; Janesko, B. G.; Gomperts, R.; Mennucci, B.; Hratchian, H. P.; Ortiz, J. V.; Izmaylov, A. F.; Sonnenberg, J. L.; Williams-Young, D.; Ding, F.; Lipparini, F.; Egidi, F.; Goings, J.; Peng, B.; Petrone, A.; Henderson, T.; Ranasinghe, D.; Zakrzewski, V. G.; Gao, J.; Rega, N.; Zheng, G.; Liang, W.; Hada, M.; Ehara, M.; Toyota, K.; Fukuda, R.; Hasegawa, J.; Ishida, M.; Nakajima, T.; Honda, Y.; Kitao, O.; Nakai, H.; Vreven, T.; Throssell, K.; Montgomery, J. A., Jr.; Peralta, J. E.;; Ogliaro, F.; Bearpark, M. J.; Heyd, J. J.; Brothers, E. N.; Kudin, K. N. S., V. N.;; Keith, T. A.; Kobayashi, R. N., J.; Raghavachari, K.; Rendell, A. P.;; Burant, J. C.; Iyengar, S. S.; Tomasi, J.; Cossi, M.; Millam, J. M.; Klene, M.; Adamo, C.; Cammi, R.; Ochterski, J. W.; Martin, R. L.; Morokuma, K.; Farkas, O.; Foresman, J. B.; Fox, D. J. *Gaussian 16, revision A.03*, Gaussian, Inc.: Wallingford, CT, 2016.

70. Jorgensen, W. L.; Chandrasekhar, J.; Madura, J. D.; Impey, R. W.; Klein, M. L., Comparison of Simple Potential Functions for Simulating Liquid Water. *J Chem Phys* **1983,** *79* (2), 926-935.

71. Izaguirre, J. A.; Catarello, D. P.; Wozniak, J. M.; Skeel, R. D., Langevin stabilization of molecular dynamics. *J Chem Phys* **2001,** *114* (5), 2090-2098.

72. Berendsen, H. J. C.; Postma, J. P. M.; Vangunsteren, W. F.; Dinola, A.; Haak, J. R., Molecular dynamics with coupling to an external bath. *J Chem Phys* **1984,** *81* (8), 3684-3690.

73. Darden, T.; York, D.; Pedersen, L., Particle mesh Ewald: An *N*·log(*N*) method for Ewald sums in large systems. *J Chem Phys* **1993,** *98* (12), 10089-10092.

74. Kräutler, V.; Van Gunsteren, W. F.; Hünenberger, P. H., A fast SHAKE: Algorithm to solve distance constraint equations for small molecules in molecular dynamics simulations. *J Comput Chem* **2001,** *22* (5), 501-508.

75. Götz, A. W.; Williamson, M. J.; Xu, D.; Poole, D.; Le Grand, S.; Walker, R. C., Routine Microsecond Molecular Dynamics Simulations with AMBER on GPUs. 1. Generalized Born. *J Chem Theory Comput* **2012,** *8* (5), 1542-1555.

76. Salomon-Ferrer, R.; Case, D. A.; Walker, R. C., An overview of the Amber biomolecular simulation package. *Wires Comput Mol Sci* **2013,** *3* (2), 198-210.

77. Salomon-Ferrer, R.; Götz, A. W.; Poole, D.; Le Grand, S.; Walker, R. C., Routine Microsecond Molecular Dynamics Simulations with AMBER on GPUs. 2. Explicit Solvent Particle Mesh Ewald. *J Chem Theory Comput* **2013,** *9* (9), 3878-3888.

78. Metz, S.; Kästner, J.; Sokol, A. A.; Keal, T. W.; Sherwood, P., ChemShell-a modular software package for QM/MM simulations. *Wires Comput Mol Sci* **2014,** *4* (2), 101-110.

79. Neese, F., The ORCA program system. *Wires Comput Mol Sci* **2012,** *2* (1), 73-78.

80. Neese, F., Software update: The ORCA program system-Version 5.0. *Wires Comput Mol Sci* **2022,** *12* (5), e1606.

81. Smith, W.; Forester, T. R., DL_POLY_2.0: A general-purpose parallel molecular dynamics simulation package. *J Mol Graphics* **1996,** *14* (3), 136-141.

82. Smith, W., DL_POLY-applications to molecular simulation II. *Mol Simulat* **2006,** *32* (12-13), 933-933.

83. Bakowies, D.; Thiel, W., Hybrid models for combined quantum mechanical and molecular mechanical approaches. *J Phys Chem-Us* **1996,** *100* (25), 10580-10594.

84. Runge, E.; Gross, E. K. U., Density-Functional Theory for Time-Dependent Systems. *Physical Review Letters* **1984,** *52* (12), 997-1000.

85. Yanai, T.; Tew, D. P.; Handy, N. C., A new hybrid exchange-correlation functional using the Coulomb-attenuating method (CAM-B3LYP). *Chemical Physics Letters* **2004,** *393* (1-3), 51-57.

86. Lee, C. T.; Yang, W. T.; Parr, R. G., Development of the Colle-Salvetti Correlation-Energy Formula into a Functional of the Electron-Density. *Phys Rev B* **1988,** *37* (2), 785-789.

87. Becke, A. D., Density-Functional Thermochemistry .3. The Role of Exact Exchange. *J Chem Phys* **1993,** *98* (7), 5648-5652.

88. Zhao, Y.; Truhlar, D. G., The M06 suite of density functionals for main group thermochemistry, thermochemical kinetics, noncovalent interactions, excited states, and transition elements: two new functionals and systematic testing of four M06-class functionals and 12 other functionals. *Theoretical Chemistry Accounts* **2008,** *120* (1-3), 215-241.

89. Chai, J.-D.; Head-Gordon, M., Long-range corrected hybrid density functionals with damped atom-atom dispersion corrections. *Phys Chem Chem Phys* **2008,** *10* (44), 6615-6620.

90. Adamo, C.; Barone, V., Toward reliable density functional methods without adjustable parameters: The PBE0 model. *J Chem Phys* **1999,** *110* (13), 6158-6170.

91. Cossi, M.; Barone, V., Time-dependent density functional theory for molecules in liquid solutions. *J Chem Phys* **2001,** *115* (10), 4708-4717.

92. Mennucci, B.; Tomasi, J., Continuum solvation models: A new approach to the problem of solute's charge distribution and cavity boundaries. *J Chem Phys* **1997,** *106* (12), 5151-5158.
93. Lu, T.; Chen, F. W., Multiwfn: A multifunctional wavefunction analyzer. *J Comput Chem* **2012,** *33* (5), 580-592.
94. Humphrey, W.; Dalke, A.; Schulten, K., VMD: Visual molecular dynamics. *J Mol Graph Model* **1996,** *14* (1), 33-38.
95. Delano, W. L., Pymol: an open-source molecular graphics tool. *CCP4 Newsl. Protein Crystallogr.* **2002,** *40*, 82-92.
96. Liu, Z. Y.; Lu, T.; Chen, Q. X., An sp-hybridized all-carboatomic ring, cyclo[18]carbon: Electronic structure, electronic spectrum, and optical nonlinearity. *Carbon* **2020,** *165*, 461-467.
97. Noguchi, Y.; Hiyama, M.; Shiga, M.; Akiyama, H.; Sugino, O., Photoabsorption Spectra of Aqueous Oxyluciferin Anions Elucidated by Explicit Quantum Solvent. *J Chem Theory Comput* **2019,** *15* (10), 5474-5482.
98. Chen, S. F.; Yue, L.; Liu, Y. J.; Lindh, R., Multireference Theoretical Studies on the Solvent Effect of Firefly Multicolor Bioluminescence. *Int J Quantum Chem* **2011,** *111* (13), 3371-3377.
99. Wang, Z. F.; Danovich, D.; Ramanan, R.; Shaik, S., Oriented-External Electric Fields Create Absolute Enantioselectivity in Diels-Alder Reactions: Importance of the Molecular Dipole Moment. *J Am Chem Soc* **2018,** *140* (41), 13350-13359.
100. Shaik, S.; Danovich, D.; Joy, J.; Wang, Z. F.; Stuyver, T., Electric-Field Mediated Chemistry: Uncovering and Exploiting the Potential of (Oriented) Electric Fields to Exert Chemical Catalysis and Reaction Control. *J Am Chem Soc* **2020,** *142* (29), 12551-12562.
101. Rebane, A.; Makarov, N. S.; Drobizhev, M.; Spangler, B.; Tarter, E. S.; Reeves, B. D.; Spangler, C. W.; Meng, F. Q.; Suo, Z. Y., Quantitative prediction of two-photon absorption cross section based on linear spectroscopic properties. *J Phys Chem C* **2008,** *112* (21), 7997-8004.
102. Drobizhev, M.; Tillo, S.; Makarov, N. S.; Hughes, T. E.; Rebane, A., Color Hues in Red Fluorescent Proteins Are Due to Internal Quadratic Stark Effect. *J Phys Chem B* **2009,** *113* (39), 12860-12864.
103. Lu, T.; Chen, Q., Ultrastrong Regulation Effect of the Electric Field on the All-Carboatomic Ring Cyclo 18 Carbon. *Chemphyschem* **2021,** *22* (4), 386-395.
104. Stanton, J. F.; Bartlett, R. J., The Equation of Motion Coupled-Cluster Method - a Systematic Biorthogonal Approach to Molecular-Excitation Energies, Transition-Probabilities, and Excited-State Properties. *J Chem Phys* **1993,** *98* (9), 7029-7039.
105. Wang, Z. F.; Feng, S. S.; Rovira, C.; Wang, B. J., How Oxygen Binding Enhances Long-Range Electron Transfer: Lessons From Reduction of Lytic Polysaccharide Monooxygenases by Cellobiose Dehydrogenase. *Angew Chem Int Edit* **2021,** *60* (5), 2385-2392.
106. Wu, L.; Wang, Z. F.; Cen, Y. X.; Wang, B. J.; Zhou, J. H., Structural Insight into the Catalytic Mechanism of the Endoperoxide Synthase FtmOx1. *Angew Chem Int Edit* **2022,** *61* (12), e202112063.
107. Wang, B. J.; Cao, Z. X.; Rovira, C.; Song, J. S.; Shaik, S., Fenton-Derived OH Radicals Enable the MPnS Enzyme to Convert 2-Hydroxyethylphosphonate to Methylphosphonate: Insights from Ab Initio QM/MM MD Simulations. *J Am Chem Soc* **2019,** *141* (23), 9284-9291.
108. Ali, H. S.; Warwicker, J.; de Visser, S. P., How Does the Nonheme Iron Enzyme NapI React through l-Arginine Desaturation Rather Than Hydroxylation? A Quantum Mechanics/Molecular Mechanics Study. *Acs Catal* **2023,** *13* (16), 10705-10721.
109. Kabir, M. P.; Ouedraogo, D.; Orozco-Gonzalez, Y.; Gadda, G.; Gozem, S., Alternative Strategy for Spectral Tuning of Flavin-Binding Fluorescent Proteins. *J Phys Chem B* **2023,** *127* (6), 1301-1311.

Table of Contents